RSC Advances

PAPER

View Article Online
View Journal | View Issue

Cite this: *RSC Adv.*, 2019, **9**, 17473

Shape-controllable nanofibrous membranes with well-aligned fibers and robust mechanical properties for $PM_{2.5}$ capture†

Jian Chen,‡[a] Zhiqiang Cheng,*[b] Yafeng Yuan,[b] Jingjing Zhang[b] and Jinshan Cao‡*[b]

In this study, design and fabrication of novel shape-controllable and aligned nanofibrous membranes with self-cleaning and robust mechanical properties is presented. Smooth and uniform nanofibers can be fabricated by blending polyamide 66 (PA66) and poly (vinyl butyral) (PVB) with a mass ratio of 6/4 during electrospinning. Subsequently, the prepared nanofibrous membranes were placed in a vacuum drying oven at a given temperature (90 °C) for heat treatment, and the morphology of the composite nanofibers was controlled by an external tensile force. It was found that the treatment temperature and external tensile force greatly affected the pore structures and orientation of the nanofiber membranes. In addition, the hydrophobicity, pore structure and mechanical properties of well-aligned nanofibrous membranes are better than those of non heat-treatment nanofibers. Moreover, the PA66/PVB nanofibrous membranes are used as air filters, and show an excellent removal efficiency of up to 99.99% for $PM_{2.5}$.

Received 27th March 2019
Accepted 13th May 2019

DOI: 10.1039/c9ra02341k

rsc.li/rsc-advances

1 Introduction

With the rapid development of the social economy, for the majority of developing countries and the undeveloped region, increasing air pollution has become the primary concern in recent years.[1] The concentration of pollutants in many cities has been in excess of standards for a long time, and many cities have ambient levels of $PM_{2.5}$ far above the Air Quality Guideline ($\leq$10 μg m^{-3}) established by the World Health Organization (WHO).[2] $PM_{2.5}$ (atmospheric particulate matter that has a diameter of less than or equal to 2.5 μm in aerodynamic diameter[3]) contains a large number of toxic and harmful particles, which have a significant impact on human health[4] and social production.[5] Inhaling $PM_{2.5}$ can lead to diseases such as asthma,[6] chronic bronchitis[7] and cardiovascular diseases.[8] In addition, the main source of $PM_{2.5}$ is the residue from combustion in daily power generation, automobile exhaust emission and so on. The Global Environment Outlook 5 (GEO-5), released by the United Nations Environment programme in 2012, indicated that nearly 2 million premature deaths are linked to particulate pollution. Proceedings of the National Academy of Sciences of the United States of America (PNAS) also reported that human life expectancy is likely to have been shortened by five and a half years due to excessive inhalation of airborne particulate matter.

Currently, common air filtration technologies includes the cottrell process, electrostatically stimulated fabric filtration (ESFF),[9] stretch film technology[10] and efficient fiber filtration technology.[11] Efficient fiber filtration technology has become a research focus due to the many advantages such as strong structural adjustability. Among the various methods used to prepare nanofibers, electrospinning technology can obtain nanofibers with a high specific surface area due to the simple operation, large output, and controllable fiber diameter.[12] Furthermore, electrospun nanofibers have high porosity[13] and excellent flexibility,[14] and thereby have been extensively used in engineering materials,[15] catalysis,[16] filtration,[17] bioengineering scaffolds, drug delivery,[18] wound suture and optoelectronic devices.[19]

However, single polymer nanofibrous membranes often have some performance defects, and the modification of nanofibers by appropriate methods can greatly improve the overall performance of materials. Polymer blending is one of the important modification methods.[20] Both PA66 and PVB are widely used thermoplastic resins and there is a great difference in melting point between them. The melting point of PA66 is about 250 °C.[21] However, as a type of special thermoplastic polymer, the softening temperature of PVB is 60–65 °C and the glass transition temperature is 66–90 °C.[22] Besides, there are few reports on further treatment of the nanofibers by heating induced phase transition after blending.

[a]*Institute of Environmental Toxicology and Environmental Ecology, Institute of New Energy on Chemical Storage and Power Sources, College of Chemistry and Environmental Engineering, Yancheng Teachers University, Yancheng 224007, China*
[b]*College of Resources and Environment, Jilin Agricultural University, Changchun 130118, China. E-mail: czq5974@163.com; cjs4451@126.com*

† Electronic supplementary information (ESI) available. See DOI: 10.1039/c9ra02341k

‡ Jian Chen and Jinshan Cao contributed to this work equally.

In this paper, shape-controllable PA66/PVB composite nanofibrous membranes were prepared by controlling the heat treatment temperature, and external tension is applied to regulate the structure of the membranes during heat treatment. Moreover, PA66/PVB composite fibrous membranes with well-aligned fibers have robust mechanical properties compared to other samples. The morphology of the samples was observed by SEM. Subsequently, the structure of the nanofibers was characterized by TGA, DSC and FTIR, and the pore size distribution, wettability and mechanical properties of the NFs were investigated. Finally, the PA66/PVB composite nanofibrous membranes were placed in a home-built device, and the removal efficiency for $PM_{2.5}$ was tested in a simulated polluted environment.

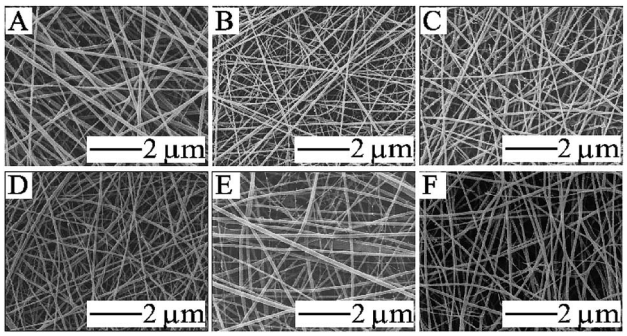

Fig. 1 SEM images of electrospun nanofibers with different mass ratios of PA66/PVB: (A) 5/5; (B) 6/4; (C) 7/3; (D) 8/2; (E) 9/1; (F) pure PA66.

2 Experiment section

2.1 Materials

Polyamide 66 (PA66, EPR-27) white granules and poly (vinyl butyral) (PVB, molecular weight (MW) ranging from 170, 000 to 250, 000 g mol^{-1}) were purchased from Tianjing Bodi Chemical Co., Ltd. and Sinopharm Chemical Reagent Co., Ltd, respectively. Formic acid (99%, F112036, Analytical Regent) was obtained from Shanghai Aladdin Bio-Chem Technology Co., Ltd. All reagents are the highest commercially available grade and used as received without further purification.

2.2 Fabrication of nanofibrous membranes

Scheme 1 shows the forming process of shape-controllable nanofibrous membranes. Firstly, the solution was prepared by dissolving the dried PA66 and PVB white granules in formic acid at an advisable concentration. The PA66 solution was stirred at 60 °C for 3 hours, and the PVB solution stirred at 30 °C for 2 hours. Then, the two solutions were mixed and stirred at 30 °C for 4 hours to achieve uniform and transparent precursor solutions.

Secondly, the precursor solution is moved into the syringe (the range is 5 mL) and placed on the propulsion plant with a programmable syringe pump. The solution flow rate is set to 0.3 mL h^{-1}. The specific parameters of the electrospinning process are as follows: the applied voltage was 18 kV, the tip-collector distance was 25 cm, the relative humidity was ~50% and room temperature was 22 °C. The nozzle used in the experiment has an inner diameter of 0.6 mm. Simultaneously, the generated nanofibers were collected by a metallic rotating roller with a rotation rate of 300 rpm.

The melting point of PVB is relatively low compared with that of PA66, thus when the treatment temperature is higher than the melting point of PVB, PVB begins to melt while the PA66 nanofibers still maintain their complete structure as supporting materials. We can effectively optimize the optimum conditions by adjusting the mass ratio of PA66 and PVB. The mass ratio of PA66/PVB was adjusted to 5/5, 6/4, 7/3, 8/2 and 9/1 (Fig. 1). Finally, the PA66/PVB composite nanofibrous membranes obtained under the optimum parameter were cut into rectangular strips of the same size, heated under different temperatures (as shown in Fig. S1†) and hung in a vacuum drying oven, and the treatment time is 4 hours. In addition, weights of 0 g, 5 g, 10 g and 15 g were clamped at the bottom of the samples as the external tensile force. The results showed that the morphology and structure of the PA66/PVB nanofibrous membranes were affected by the external tensile force during heat treatment (Fig. 2A–D). In this paper, the as-prepared samples after heat treatment were named W-5G, W-10G and W-15G nanofibrous membranes, respectively.

2.3 Characterization

2.3.1 Morphology and fiber diameter. The surface morphology of the samples was characterized using a scanning electron microscope (SEM, SHIMADZU X-550, Japan, operating

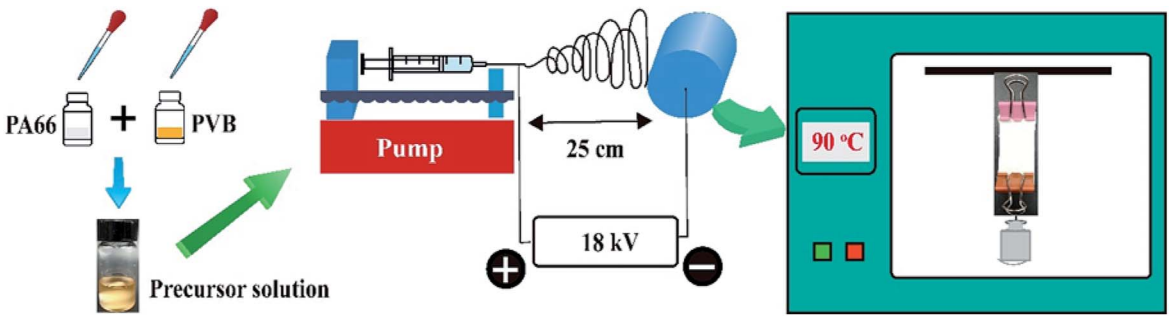

Scheme 1 Schematic presenting the forming process of the shape-controllable nanofibrous membranes.

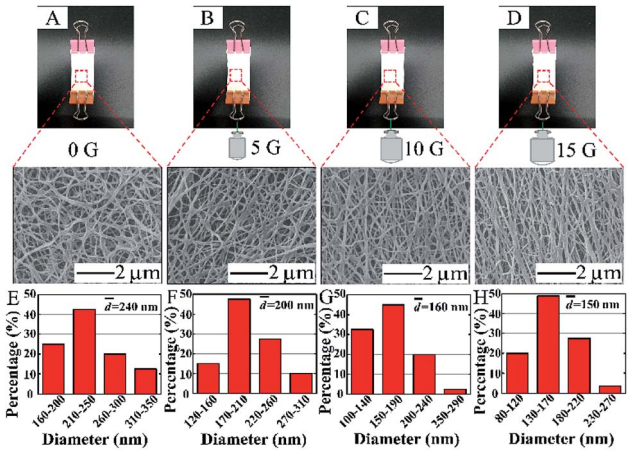

Fig. 2 Digital photos and SEM images of the obtained nanofibers at the mass ratio of 6/4 with different external tensile forces: (A) 0 g; (B) 5 g; (C) 10 g; (D) 15 g. (E–H) The corresponding distribution of fiber diameters of the PA66/PVB nanofibrous membranes.

voltage: 15 kV). Furthermore, the fiber diameter distribution was determined manually from the SEM images using the Nanomeasure 1.2 software.

2.3.2 Structure analysis and thermal properties. Fourier transform infrared (FTIR) spectra were obtained from the Paragon 1000 Spectrometer (PerkinElmer) at a signal resolution of 1 cm^{-1} within the range of 400–4000 cm^{-1}.

The pore size distribution of the samples was measured using a membrane pore size analyzer based on a bubble point method (3H-2000PB, Beishide Instrument Technology Co., Ltd).

The thermal properties were obtained from TGA (HCT-3, China). Under an air atmosphere, the TGA was conducted over a temperature range of 30–800 °C at a heating rate of 10 °C min^{-1}. Furthermore, the temperature for DSC was set to 30 °C–400 °C, and the heating rate was also set to 10 °C min^{-1}.

2.3.3 Wettability. The wettability was measured using a contact angle analyser (Kino SL200B, USA). In the process of characterizing the water contact angle, deionized water was selected as the liquid, and a 3 mL water droplet (diameter: ~2 mm) was dripped onto the surface of the samples from a height of 5 cm at room temperature. The water contact angles were measured three times repeatedly, and the average results were selected to represent the water contact angle of the samples.

2.3.4 Mechanical properties. The mechanical properties of the samples were measured by a mechanical testing tester (WDW-X, China). During the testing process, the loading force was 5 N and the stretching speed was 2 mm min^{-1}. 5 samples with a gauge length of 25 mm in a spindle-shaped sample (50 mm × 10 mm) from the same synthesis cycle were tested, and the averaged strain *vs.* stress performance was plotted.

2.3.5 PM generation and filtration efficiency measurement. The PM particles used in this study were generated by burning tobacco, because tobacco smoke contains a wide range of PM particles of various sizes for air filtration experiments. The number of particles through the air filters was detected by an air particle counter (MET ONE 237B, USA). The pressure drop was evaluated by an automated filter tester (TSI8130, TSI Inc., MN, USA) according to ISO 11057 (air quality, test method for filtration characterization).

The removal efficiency of air filters for PM is calculated by the following formula:

$$\eta = \frac{C_{in} - C_{out}}{C_{in}} \times 100\% \quad (1)$$

where C_{in} and C_{out} represent the cumulative mass concentration of particles at the inlet and outlet, respectively. The pressure drop (ΔP) was calculated using the reading from a differential pressure gauge (AS510, Smart Sensor Pty Ltd, China). The schematic diagram of air filtration is shown in Fig. 7A and S3.† The overall performance of the air filters, considering both removal efficiency and pressure drop, is assessed by the quality factor (QF).

$$QF = \frac{\ln(1-\eta)}{\Delta P} \quad (2)$$

where η represents the removal efficiency of PM and ΔP represents the pressure drop.

3 Results and discussion

3.1 Morphology characterizations

The PA66/PVB composite nanofibrous membranes with different mass ratios were obtained by changing the proportion of PVB in the precursor solution. Fig. 1 displays the surface morphology of the nanofibers. The morphology of electrospun nanofibers began to differ with decreasing PVB content. The PA66/PVB nanofibrous membranes with a mass ratio of 6/4 (Fig. 1B) show a uniform fiber diameter compared with other samples. Furthermore, the surface of the nanofibers is smooth and the nanofibers are evenly distributed. So we choose the PA66/PVB nanofibrous membranes with a mass ratio of 6/4 for further experiment.

PVB begins to melt when the temperature of heat treatment is higher than 65 °C, the maximum softening temperature of PVB. Besides, the PA66 nanofibers still retain their original structure, and act as the scaffold of the whole nanofibrous membrane, since the melting point of PA66 is much higher than that of PVB. Fig. 2A–D indicate the digital photos and SEM images of the obtained PA66/PVB composite nanofibrous membranes after heat treatment (90 °C). When the bottom of the membrane does not hold the weight, many pore structures are formed with the increase of the treatment temperature, and the average fiber diameter is about 240 nm. After holding the weights, the nanofibers began to present directional distribution with increasing weight, and the pore structures were also deformed. By this token, the external tensile force can greatly affect the morphology and pore structure of nanofibrous membranes. Moreover, we could find that the fiber diameter is gradually decreasing (as shown in Fig. 2E–F), thus forming shape-controllable PA66/PVB composite nanofibrous membranes with well-aligned fibers.

3.2 Structure analysis

Fig. 3 shows the FTIR spectra of PA66, PVB and the PA66/PVB nanofibrous membranes. It is apparent that the PA66 nanofibrous membranes exhibit distinct absorption peaks at 3300 cm^{-1} (N–H stretching), 1630 cm^{-1} (C=O stretching) and 1529 cm^{-1} (N–H bending), which indicates the secondary amide structure.[23] The FTIR spectrum of PVB is shown by the orange line; absorption peaks at 3431 cm^{-1} and 2956 cm^{-1} signify the stretching vibration of –OH and aliphatic C–H groups. The peak at 1731 cm^{-1} is attributed to the stretching vibration of C=O.[24] Furthermore, no new peaks appear, which indicates that there is no chemical interaction between PA66 and PVB in the nanofibrous membranes.

Fig. 4 illustrates the TGA and DSC curves of three samples. Firstly, the TGA curve of PVB was divided into two regions, and the major stage of weight loss occurred at 254 °C and is related to the OH groups – the groups are separated as water. The butyral group is degraded at 389 °C. PA66 decomposes in several stages. The major decomposition region at around 340–430 °C is attributed to the decomposition of PA66. The pure PA66 is completely decomposed around 500 °C. In addition, the thermal decomposition of the nanofibrous membranes can be further determined by DSC curves. To sum up, the thermal properties of the PA66/PVB composite nanofibers were improved compared to pure PA66 and pure PVB nanofibrous membranes.

Pore size distribution is a parameter which describes the variation of pore size in nanofibrous membranes, and is defined as the percentages of various pore sizes in terms of quantity or volume.[25] The pore structure often affects the kinetic properties of the airstream, and then regulates the air permeability of air filters and their capture ability for $PM_{2.5}$. Recently, electrospun nanofibrous membranes have attracted much attention because of their unique pore structure in the field of air filtration.[26] The pore size distribution of various samples is shown in Fig. 5. In the course of heat treatment, we also investigated the influence of the external tensile force on the pore structure of the nanofibers. The pore size distribution value of the fibers becomes smaller and the fiber diameter becomes thinner with increasing tensile force. Moreover, the results indicate an obvious difference of pore size distribution, which was attributed to the aligned structure. In addition, the average pore diameter of the W-15G nanofibrous membranes was about 0.5058 μm.

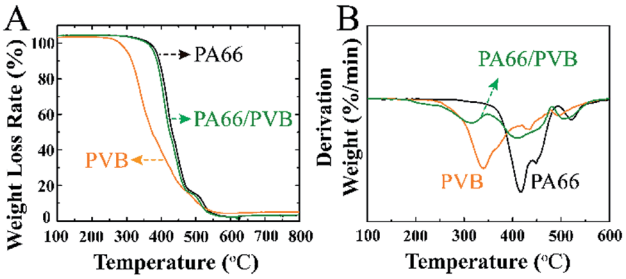

Fig. 4 (A) TGA curves of the electrospun nanofibrous membranes and (B) the corresponding DSC curves.

3.3 Wettability and mechanical properties

Excellent hydrophobicity and mechanical properties can improve the self-cleaning ability and service life of nanofibrous membranes, so the membranes can be used in a more complicated environment. Firstly, Fig. 6A indicates the water contact angle of various nanofibrous membranes with different weights. As a result, we could find that the water contact angle of the nanofibrous membranes gradually increased as the external tensile force increased, which indicates that the self-cleaning ability of the surface of the nanofibrous membranes was improved compared to other samples.

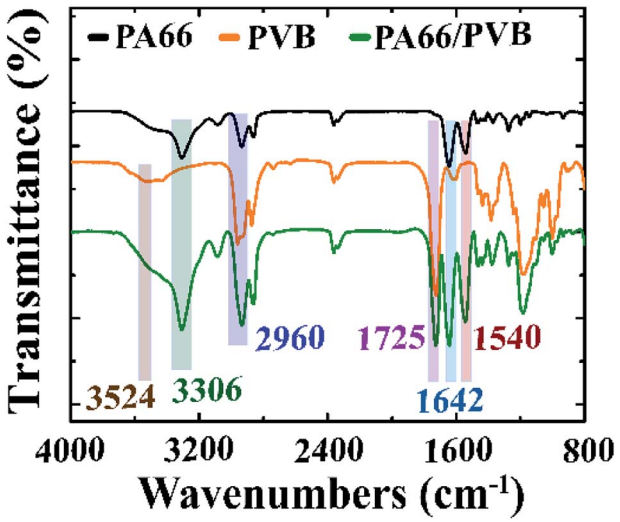

Fig. 3 FTIR spectra of PA66, PVB and the PA66/PVB nanofibrous membranes.

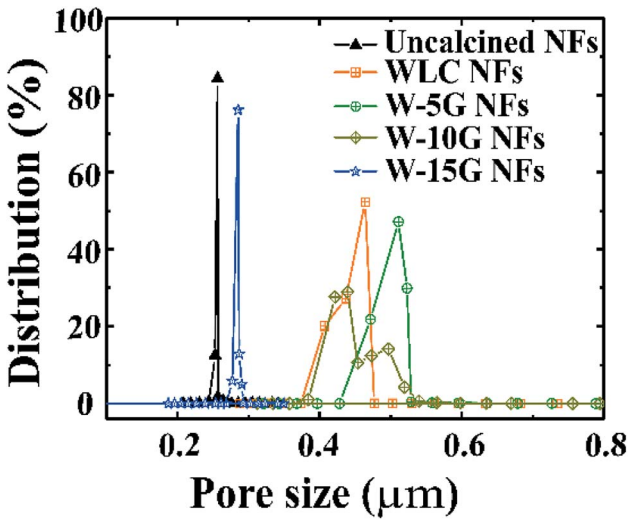

Fig. 5 Pore size distribution curves of the PA66/PVB composite nanofibrous membranes with different weights.

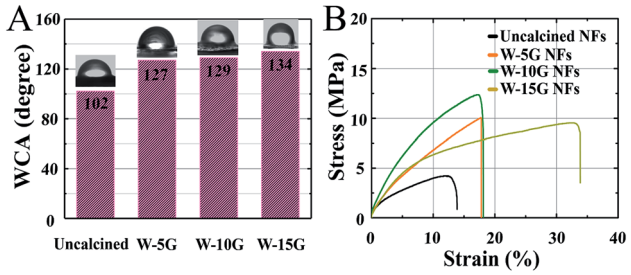

Fig. 6 (A) Water contact angle and (B) typical stress–strain curves of electrospun PA66/PVB nanofibrous membranes.

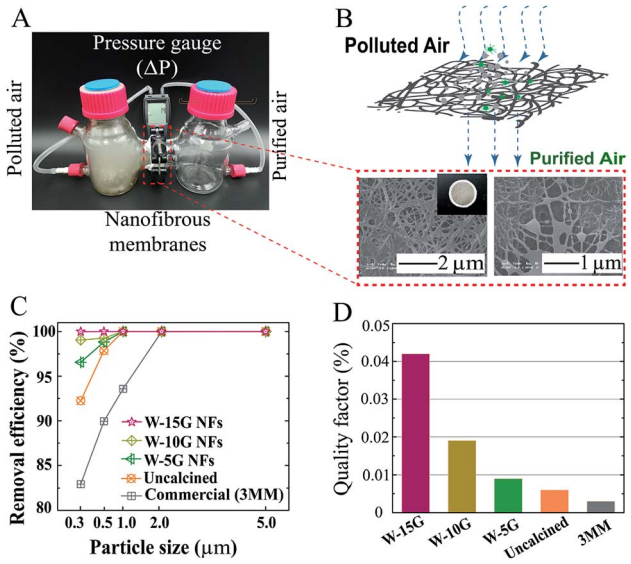

Fig. 7 (A) Schematic illustration of the setup for the measurement of the pressure drop and air filtration performance. (B) Schematics of W-15G nanofibrous membranes, with well-aligned fibers and robust mechanical properties, that capture airborne particles and SEM images showing the membrane morphology after a 24 h PM capture test. (C) The $PM_{0.3-5.0}$ removal efficiency and (D) the corresponding quality factor.

Secondly, as shown in Fig. 6B, the mechanical properties of the PA66/PVB composite nanofibrous membranes after heat treatment are superior to those of non-heat treated membranes, and the aligned nanofibers of W-15G possess an excellent tensile strength of 10.6 MPa and an elongation at break strain of 33.9%.

3.4 Evaluation of air filtration performance

Fiber filtration is an efficient technology: it uses the stacked functional fiber layer as the main material for air filtration.[27] When the diameter of the polluted particles is larger than the pore size of the fibrous membranes, the particles are filtered out due to the intercepting and filtering mechanism. If the diameter of the particles is smaller than the size of the air filter, some of the particles will be filtered out because of other mechanisms (such as electrostatic adsorption[28] or Brownian diffusion[29]). Fig. 7 and Table 1 describe the filtration efficiency of the samples under hazardous level conditions equivalent to the $PM_{2.5}$ index 200 for 24 h. Fig. 7A is the photo of the pressure drop measurement, and the pressure difference across the air filter was monitored. The nanofibrous membranes were clamped gas-tightly in the middle of an H-shaped cell. The left side simulates polluted air by burning tobacco, while the right side is purified air. The high magnification SEM images after filtration are shown in Fig. 7B. The general capture mechanism for airborne particles indicates that the particles would wrap around the nanofibers, and most dust particles are intercepted on the surface of the nanofibrous membranes. We selected commercial masks (9501C, 3M China) and the uncalcined nanofibrous membranes as comparative samples for the characterization of air filtration. Fig. 7C and D show the filtration efficiency for $PM_{0.3-5.0}$ and the quality factor of various samples. Among them, W-15G nanofibrous membranes illustrate the highest removal efficiency of up to 99.99% for $PM_{2.5}$. Furthermore, the quality factor of W-15G membranes is also the highest, which indicates that the regular oriented structure of the nanofibrous membranes has a great effect on the comprehensive filtration performance of air filters. The detailed results are listed in Table 1.

4 Conclusions

To sum up, we successfully fabricated shape-controllable and well-aligned PA66/PVB nanofibrous membranes by a facile method of electrospinning and heat-induced alignment, and the obtained nanofibrous membranes exhibit excellent hydrophobicity and mechanical properties. The optimal mass ratio of preparing PA66/PVB composite nanofibers is 6 : 4 through plenty of optimization experiments. Under the optimum treatment temperature (90 °C), the pore structures, mechanical properties and water contact angle of nanofibrous membranes are improved with the increase of the weight at the bottom of

Table 1 Detailed information of various air filters for capturing airborne particles

	Filtration efficiency (%)							
Sample	0.3 μm	0.5 μm	1.0 μm	2.0 μm	5.0 μm	Thickness/mm	Δ*P*/Pa	QF
W-15G	99.99	100	100	100	100	0.046 ± 0.002	218.30	0.042
W-10G	99.05	99.26	100	100	100	0.042 ± 0.003	238.86	0.019
W-5G	96.56	98.82	100	100	100	0.037 ± 0.002	356.21	0.009
Uncalcined	92.24	97.86	100	100	100	0.040 ± 0.003	366.98	0.006
3MM	82.94	89.95	93.58	99.99	100	0.045 ± 0.001	495.02	0.003

the membranes. The best comprehensive performance is from the W-15G nanofibrous membranes, and their average pore diameter was about 0.5058 μm. The well-aligned nanofibers were able to capture $PM_{2.5}$, showing excellent removing efficiency and the filtration efficiency for 0.3 μm reached 99.99%. We may safely conclude that shape-controllable and well-aligned PA66/PVB composite nanofibrous membranes will provide new ideas for the development of air filters.

Conflicts of interest

There are no conflicts to declare.

Acknowledgements

This work is supported by the National Natural Science Foundation of China (No. 41877118 and 51702279), the Qing-Lan Project of Jiangsu Province, Jilin Province Innovation Capacity Building Fund Project (2019C050-9), Jilin Provincial Department of Science and Technology Natural Science Foundation (20180101212JC) and the Changchun Science and Technology Project (18DY023).

References

1 J. Xu, C. Liu, P.-C. Hsu, K. Liu, R. Zhang, Y. Liu and Y. Cui, *Nano Lett.*, 2016, **16**, 1270–1275.
2 R. Zalakeviciute, Y. Rybarczyk, J. López-Villada and M. V. Diaz Suarez, *Atmos. Pollut. Res.*, 2018, **9**, 66–75.
3 Y. Gaoa, E. D. Nelsonb, M. P. Fielda, Q. Ding, H. Li, R. M. Sherrell, C. L. Gigliotti, D. A. V. Ry, T. R. Glenn and S. J. Eisenreich, *Atmos. Environ.*, 2002, **36**, 1077–1086.
4 M. Kampa and E. Castanas, *Environ. Pollut.*, 2008, **151**, 362–367.
5 K. Takahashi, K. Nansai, S. Tohno, M. Nishizawa, J.-i. Kurokawa and T. Ohara, *Atmos. Environ.*, 2014, **97**, 406–415.
6 M. Guarnieri and J. R. Balmes, *Lancet*, 2014, **383**, 1581–1592.
7 L. Bai, X. Su, D. Zhao, Y. Zhang, Q. Cheng, H. Zhang, S. Wang, M. Xie and H. Su, *J. Epidemiol. Community Health*, 2018, 1–8.
8 F. Dominici, R. D. Peng, M. L. Bell, L. Pham, A. McDermott, S. L. Zeger and J. M. Samet, *JAMA, J. Am. Med. Assoc.*, 2006, **295**, 1127–1134.
9 H. Li, Z. Wang, Y. Ye and Z. Wang, *Powder Technol.*, 2016, **291**, 499–505.
10 K. D. Dunno, J. Wyns and J. Cook, *International Journal of Advanced Packaging Technology*, 2017, **5**, 267–274.
11 S. Zhang, H. Liu, F. Zuo, X. Yin, J. Yu and B. Ding, *Small*, 2017, **13**, 1603151.
12 K. Mondal and A. Sharma, *RSC Adv.*, 2016, **6**, 94595–94616.
13 C. Kim, Y. I. Jeong, B. T. Ngoc, K. S. Yang, M. Kojima, Y. A. Kim, M. Endo and J. W. Lee, *Small*, 2007, **3**, 91–95.
14 X. Guan, G. Zheng, K. Dai, C. Liu, X. Yan, C. Shen and Z. Guo, *ACS Appl. Mater. Interfaces*, 2016, **8**, 14150–14159.
15 L. Salvatore, V. E. Carofiglio, P. Stufano, V. Bonfrate, E. Calo, S. Scarlino, P. Nitti, D. Centrone, M. Cascione, S. Leporatti, A. Sannino, C. Demitri and M. Madaghiele, *J. Healthc. Eng.*, 2018, **2018**, 6573947.
16 Y. Jiang, G. Nie, M. Chi, Z. Yang, Z. Zhang, C. Wang and X. Lu, *RSC Adv.*, 2016, **6**, 31107–31113.
17 C. Liu, P.-C. Hsu, H.-W. Lee, M. Ye, G. Zheng, N. Liu, W. Li and Y. Cui, *Nat. Commun.*, 2015, **6**, 6205.
18 T. J. Sill and H. A. von Recum, *Biomaterials*, 2008, **29**, 1989–2006.
19 J. Xue, J. Xie, W. Liu and Y. Xia, *Acc. Chem.Res.*, 2017, **50**, 1976–1987.
20 T. Xu, Z. Liang, B. Ding, Q. Feng and H. Fong, *Polymer*, 2018, **151**, 299–306.
21 H. Zou, N. Ning, R. Su, Q. Zhang and Q. Fu, *J. Appl. Polym. Sci.*, 2007, **106**, 2238–2250.
22 F. N. Nguyen and J. C. Berg, *J. Adhes. Sci. Technol.*, 2004, **18**, 1011–1026.
23 J. Charles, G. R. Ramkumaar, S. Azhagiri and S. Gunasekaran, *E-J. Chem.*, 2009, **6**, 23–33.
24 A. M. Torki, D. B. Stojanović, I. D. Živković, A. Marinković, S. D. Škapin, P. S. Uskoković and R. R. Aleksić, *Polym. Compos.*, 2012, **33**, 158–168.
25 G. A. Ferrero, K. Preuss, A. B. Fuertes, M. Sevilla and M. M. Titirici, *J. Mater. Chem. A*, 2016, **4**, 2581–2589.
26 V. V. Kadam, L. Wang and R. Padhye, *J. Ind. Text.*, 2016, **47**, 2253–2280.
27 K. M. Yun, C. J. Hogan, Y. Matsubayashi, M. Kawabe, F. Iskandar and K. Okuyama, *Chem. Eng. Sci.*, 2007, **62**, 4751–4759.
28 Q. Li, Y. Xu, H. Wei and X. Wang, *RSC Adv.*, 2016, **6**, 65275–65281.
29 H. Zhang, J. Liu, X. Zhang, C. Huang and X. Jin, *RSC Adv.*, 2018, **8**, 7932–7941.

